2021 American Control Conference (ACC)
New Orleans, USA, May 25-28, 2021

Observability-aware Target Tracking with Range Only Measurement

Demetris Coleman, Shaunak D. Bopardikar, and Xiaobo Tan

Abstract— **Often times in nonlinear systems, the control input can play a significant role in the system's observability. In this paper, we investigate the trade-off between observability and control performance for a mobile robot in target tracking, when only the distance to the target is measured. The problem is motivated by practical applications for autonomous robots when operating in GPS-denied environments. A nonlinear model predictive control (NMPC) framework is used to address the dilemma between localization and tracking, by jointly optimizing the tracking performance and an observability metric. Three measures of estimation performance are considered, including the determinant of the observability matrix, the inverse condition number of the observability matrix, and the trace of the covariance matrix in position estimation. By tuning the relative importance of the tracking objective and observation performance, we demonstrate the efficacy of the proposed NMPC approach. The trade-off is captured through two examples, one with unicycle dynamics on a plane, the other based on gliding robotic fish with complex 3D dynamics.**

I. Introduction

An important problem for autonomous robots in GPS-denied environments is localization and navigation with only range measurement. This is particularly relevant in the case of underwater vehicles, which have become valuable for a myriad applications [1], [2]. In particular, the subset of AUVs dubbed Underwater Gliders, has shown great promise for long-term missions [3]–[5]. AUVs, however, have significant challenges that accompany their operation. These challenges mainly stem from the underwater environment practically prohibiting many radio frequency-based solutions to localization, navigation, and communication. In addition, techniques like simultaneous localization and mapping are not always applicable due to a lack of landmarks.

Advancements in technologies available for the underwater environment offer several approaches to localization and navigation [6]. Acoustic modems, such as the micromodem developed by Woods Whole Oceanographic Institute, can provide communication and ranging between underwater vehicles or beacons. Due to the capabilities of acoustic modems, many researchers began a general study of using static beacons or surface vehicles as communication and navigation aids (CNAs) to underwater vehicles [7]–[12]. A particularly interesting instance of this class of problems is the single beacon navigation (SBN) problem and its variants. In the SBN problem, an AUV estimates its position using inertial sensors, knowledge of its dynamic model, and the measurement of its range to a single beacon while locomoting.

Several works have studied the observability of the SBN problem using a variety of methods. In [13], the authors optimize the condition number of the empirical observability Gramian in path planning to improve observability of a uniform flow field. The authors of [14] study the observability of SBN with the kinematic model of an AUV moving in the horizontal plane and a static beacon. Using the range and bearing, the authors give an explanation of when the position of the vehicle can be found using only measurements of range. The authors in [15] investigate the relative pose estimation based on range measurements between two robots moving in a 3D environment. They consider only the kinematic model. The authors of [16] study the observability of relative localization of two AUVs equipped with velocity, depths sensors, and ranging capability. The authors derive an observability metric and show that the degradation of localization performance depends on the range between the vehicles and the angle between the relative velocity vector and the position vector. In [17], the authors argue that optimizing measures of the observability Gramian as a surrogate for the estimation performance may provide irrelevant or misleading trajectories for planning under observation uncertainty. The authors instead suggest using measures of the Posterior Fisher Information Matrix. As an example, they use the trace of the covariance matrix produced by a Kalman filter.

Most of these works focus on localization, navigation, or path planning. Comparatively, work on control based on observability metrics in the context of range measurement has been limited. The authors of [18] developed a controller for homing in on a static beacon using range measurements. The controller was inspired by previous results on observable paths, but used a heuristic approach based on a covariance threshold to achieve observable maneuvers. One notable exception is [19], where the authors present two methods of greedy-optimal steering control for CNAs. The authors consider the AUVs as static beacons and use approximate optimization of the condition number of the observability Gramian to steer the CNAs improving localization for underwater vehicles.

The work cited above typically has not considered the relative importance between an observability metric and a tracking objective. This work differentiates itself from existing work in this area by studying the application of observability-based control to the target tracking problem. We consider an underwater vehicle tasked with tracking

The work was supported in part by National Science Foundation (IIS 1848945, ECCS 2030556) and and Department of Education (Grant # P200A180025).

Demetris Coleman Shaunak Bopardikar, and Xiaobo Tan are with the Department of Electrical and Computer Engineering, Michigan State University, East Lansing, MI 48824, USA. Email: colem404@msu.edu (D.C.), shaunak@egr.msu.edu (S.B), xbtan@egr.msu.edu (X.T)

the CNA using only range measurement. This scenario can arise in long-duration missions over large areas. The vehicle could surface frequently to maintain tracking performance using GPS fixes, but this would consume more energy. An alternative approach is to use a single surface vessel as a CNA, allowing the vehicle to surface less often, save energy, and stay stealthy. It has been heavily reported that traveling in a straight line toward the target lacks observability when estimating position using only range measurements [16], [19], [20]. This can be avoided by maximizing the tracking control objective together with a metric that serves as a surrogatefor estimation performance, ultimately benefiting control performance. In particular, we propose the use of NMPC to jointly optimize tracking control performance and an observability metric. We then focus on three different metrics and investigate their utility and suitability for improving observability. We further examine the trade-off between the tracking performance and estimation accuracy as the weighting function for the two objectives is tuned. Two examples, a unicycle in 2D space and a gliding robotic fish in 3D space, are used to illustrate the proposed method.

The rest of this paper is organized as follows. Section II introduces the problem formulation. Section III reviews some concepts of observability, examines the metrics used to optimize observability, and provides analysis for two example systems. Simulation results are presented in Section IV followed by concluding remarks in Section V.

II. Problem Formulation

In this work, we consider the problem of target tracking given the measurement of range to the target. The objective is to find a sequence of control inputs or actions that improve the observability of the tracker's location, while simultaneously achieving the goal of tracking the target's position. We assume that the target's absolute location is communicated to the tracker, a good estimate of initial relative position is given, and the range to the target is measured. We also assume that the tracker is able to measure or estimate its own full state vector with the exception of position. Given the target's position $x_{ta}(t)$, $y_{ta}(t)$ in real time, we desire to minimize the error between the target and tracker positions.

In this work, we propose to optimize observability metrics along with achieving the tracking objective. We then study the trade-off between tracking control and optimizing the observability metric. We define

$$\tau_e(t) = \begin{bmatrix} x - x_{ta}(t) \\ y - y_{ta}(t) \end{bmatrix} \tag{1}$$

as the tracking error between the target and tracker planar positions (x_{ta}, y_{ta}) and (x, y). The tracker is a general nonlinear agent with state X, control input U, dynamics

$$\dot{X} = f(X, U), \tag{2}$$

and a nonlinear measurement function

$$h = \begin{bmatrix} ||\tau_e|| \\ L(X) \end{bmatrix} \tag{3}$$

where $L(X)$ is the state vector with the exception of the position. We formulate a constrained optimization problem as:

$$\min_{U} \quad J = \int_{T_0}^{T_1} \alpha||\tau_e||^2 + (1-\alpha)O dt$$

subject to the dynamics (2),

$$\begin{aligned} &\Delta U_{min} \leq \Delta U \leq \Delta U_{max} \\ &U_{min} \leq U \leq U_{max} \end{aligned} \tag{4}$$

where O is a function that measures observability, ΔU is the vector of control input rates, and α is design parameter that tunes the relative emphasis between the control objective and observability metric. Setting α to one reverts to a pure tracking problem, while $\alpha = 0$ leads to only optimizing the observability metric O.

III. Observability Metrics and Analysis

A. Nonlinear Observability Rank Condition

Before diving into the observability metrics, we briefly review the concept of the nonlinear observability rank condition. Given a general nonlinear system modeled by

$$\begin{cases} x = f(x, u) \\ y = h(x), \end{cases} \tag{5}$$

with state $x \in R^n$, input $u \in R^i$, and output $y \in R^o$, observability can be studied using the concept of local weak observability introduced in [21]. By defining the Lie derivatives of the output vector $h(x)$ as

$$\begin{aligned} &\mathcal{L}_f^0 h = h, \\ &\mathcal{L}_f^1 h = \nabla_x h f, \\ &\mathcal{L}_f^2 h = \nabla_x [\mathcal{L}_f^1 h] f, \\ &\mathcal{L}_f^n h = \nabla_x [\mathcal{L}_f^{n-1} h] f, \end{aligned} \tag{6}$$

and the nonlinear observability matrix for the system in Eq. (5), evaluated at $X = x_1$, can be constructed as

$$\mathcal{O} = \begin{bmatrix} \nabla_x \mathcal{L}_f^0 h \\ \nabla_x \mathcal{L}_f^1 h, \\ \vdots \\ \nabla_x \mathcal{L}_f^l h \end{bmatrix} \tag{7}$$

for some positive integer l. The observability rank condition for nonlinear systems states that the system (5) is locally weakly observable at x_1 if there exists an input, u, such that the matrix $\mathcal{O}(x_1, u)$ is full rank.

B. Observability Optimization Metrics

Following the conventions in [16], we study the observability of the relative position system in a general sense. Consider the evolution of the relative position of the system, $\dot{X}_r = V_r$, where V_r is the relative velocity of the system that

can be expressed as a function of the state and control. The relative state can be expressed as

$$\begin{bmatrix} X_r \\ V_r \end{bmatrix} = \begin{bmatrix} \begin{bmatrix} x_r \\ y_r \end{bmatrix} \\ \begin{bmatrix} v_{xr} \\ v_{yr} \end{bmatrix} \end{bmatrix} = \begin{bmatrix} x - x_{ta} \\ y - y_{ta} \\ \dot{x} - v_{x_{ta}} \\ \dot{y} - v_{y_{ta}} \end{bmatrix} \tag{8}$$

This simplifies the analysis by allowing the study of a time-invariant system rather than a time-varying one.

In addition, rather than studying the observability based on range measurement $||\tau_e(t)||$, we use $\frac{1}{2}||\tau_e(t)||^2$, to simplify computations while keeping the same observability properties. Taking the system as

$$\begin{cases} \dot{X}_r = V_r \\ h = \frac{1}{2}||\tau_e(t)||^2 = x_r^2 + y_r^2 \end{cases} \tag{9}$$

the observability matrix becomes

$$\mathcal{O}_p = \begin{bmatrix} \nabla \mathcal{L}_f^0 h \\ \nabla \mathcal{L}_f^1 h \end{bmatrix} = \begin{bmatrix} x_r & y_r \\ v_{xr} & v_{yr} \end{bmatrix} \tag{10}$$

A necessary and sufficient condition for $\mathcal{O}_p$ to be full rank is $\det(\mathcal{O}_p) \neq 0$. In particular, $\mathcal{O}_p$ loses rank if both relative positions are zero or both relative velocities are zero.

We consider two commonly used observability metrics based on the observability matrix and a more recent metric using the posterior probability of the estimation error in the Extended Kalman Filter as proposed in [17]. The metrics are the inverse condition number of the observability matrix C^{-1}, the determinant of the observability matrix $\det(\mathcal{O}_p)$, and the trace of the covariance matrix of the position estimate. An expression for condition number was derived in [16] by rewriting $\mathcal{O}_p$ in polar coordinates as

$$\mathcal{O}_p = \begin{bmatrix} ||X_r|| \sin(\alpha) & ||X_r|| \cos(\alpha) \\ ||V_r|| \sin(\beta) & ||V_r|| \cos(\beta) \end{bmatrix} \tag{11}$$

and defining the variables $\gamma = \frac{||X_r||}{||V_r||}$ and $\theta = \beta - \alpha = (\pi - \arctan(\frac{v_{yr}}{v_{xr}})) - (\pi - \arctan(\frac{yr}{xr}))$. The inverse condition number can be calculated

$$C^{-1} = \frac{2\gamma |\sin(\theta)|}{\gamma^2 + 1 + \sqrt{\gamma^4 + 2\gamma^2 \cos(2\theta) + 1}}. \tag{12}$$

The determinant can be expressed as

$$\det(\mathcal{O}_p) = v_{yr} x_r - v_{xr} y_r. \tag{13}$$

The trace of the estimation error covariance will be based on an EKF using range measurements. The estimation error covariance will be denoted by P.

With these three metrics, we define the cost functions O_i to be used in the optimization problem (4). They are:

$$\begin{aligned} O_1 &= -C^{-1} \\ O_2 &= -\det(\mathcal{O}_p)^2 \\ O_3 &= \mathrm{Tr}(P) \end{aligned} \tag{14}$$

C. Discussion of Metrics

Each of the three metrics have advantages and drawbacks. The observability matrix is a system property and does not rely on any particular estimation scheme. So optimizing metrics related to it should produce a state trajectory that provides optimal measurements for reconstructing the state, enhancing performance of any estimation scheme. Using metrics of the observability matrix requires not only the relative position information, but also the relative velocity between the two vehicles. Neither measure of the observability matrix accounts for uncertainty in the estimated states. This could be a problem when using those states in the optimization.

On the other hand, the EKF would only need the range measurement and state estimate to obtain an estimation error covariance, but the covariance evolution depends on the design of the filter. In addition, the EKF uses repeated linearization steps in order to estimate the error covariance. This produces a Gaussian ellipse to estimate the distribution of possible positions of the tracker, which is in reality a circle with width given by the variance of the range measurement.

For a static target, maximizing $\det(\mathcal{O}_p)^2$ alone will result in an outward spiral. This can be seen by expressing it in terms of $||X_r||$, $||V_r||$, and θ as

$$\det(\mathcal{O}_p) = ||V_r|| \cdot ||X_r|| \sin(\theta) \tag{15}$$

For a constant $||V_r||||X_r||$, a maximum exists at $\theta = \pm\frac{\pi}{2}$. Increasing it further requires maximizing $||V_r||||X_r||$. This outward spiral is actually detrimental to the observability in the long run since it degrades with range as measured by the inverse condition number C^{-1} [16]. If we express C^{-1} in terms of $||X_r||$, $||V_r||$, and θ, we obtain

$$\begin{aligned} C^{-1} &= \frac{2||V_r||||X_r|| |\sin(\theta)|}{||X_r||^2 + ||V_r||^2 + \Gamma} \\ \Gamma &= \sqrt{||X_r||^4 + 2(||V_r||||X_r||)^2 \cos(2\theta) + ||V_r||^4} \end{aligned} \tag{16}$$

It is clear that C^{-1} is a sort of normalization of $|\det(\mathcal{O}_p)|$. Due to the normalizing factor in the inverse condition number, the outward spiral may be mitigated. However, when optimizing the cost function $J = \alpha||\tau_e(t)||^2 - (1-\alpha)C^{-1}$, the term $-C^{-1} < 1$ has the drawback that for $|\alpha||\tau_e(t)||^2|$ much greater than $|(1-\alpha)C^{-1}|$, there is an increased risk of poor tracking performance due to the observability metric having less influence on the resulting control. Minimizing $\mathrm{Tr}(P)$ potentially faces the same problem, particularly if the estimation error covariance is small compared to the distance. However, $\det(\mathcal{O}_p)^2 = ||V_r||^2||X_r||^2 \sin^2(\theta)$ will grow and shrink relative to $||\tau_e(t)||^2$. This is an advantage because it will not be dominated due to the position error growing large, but it can be a drawback since the metric will vanish along with the tracking error.

D. Unicycle Analysis

The unicycle model is used to model various vehicles moving on a 2-D plane. It also provides simple dynamics, allowing more intuitive insight into the different metrics.

Therefore, to show the efficacy of the proposed approach, we take the unicycle model with relative position whose state is $[x_r, y_r, \psi]$ and has the system model

$$\begin{cases} \dot{X} = \begin{bmatrix} u_1 \cos(\psi) - v_{x_{ta}} \\ u_1 \sin(\psi) - v_{y_{ta}} \\ u_2 \end{bmatrix} \\ h = \begin{bmatrix} ||\tau_e(t)|| \\ \psi \end{bmatrix} \end{cases} \tag{17}$$

The inputs are both the speed, u_1, and the turn rate, u_2, as opposed to assuming constant speed as in previous work [13], [19]. Replacing $||\tau_e(t)||$ with $\frac{1}{2}||\tau_e(t)||^2$ and constructing the observability matrix as described in Section III-A, with terms up to $\mathcal{L}_f^3 h$, yields

$$\mathcal{O} = \begin{pmatrix} x_r & y_r & 0 \\ 0 & 0 & 1 \\ u_1 \cos(\psi) - v_{x_{ta}} & u_1 \sin(\psi) - v_{y_{ta}} & \dots \\ 0 & 0 & 0 \\ -u_1 u_2 \sin(\psi) & u_1 u_2 \cos(\psi) & \dots \\ 0 & 0 & 0 \\ -u_1 {u_2}^2 \cos(\psi) & -u_1 {u_2}^2 \sin(\psi) & \dots \\ 0 & 0 & 0 \end{pmatrix} \tag{18}$$

where the ellipsis represent non-zero terms that are inconsequential to the rank of $\mathcal{O}$. It is easy to see that a non-zero speed and turn rate will render the system observable, but beyond this, there is no clear design strategy to pick the control law. According to section III-B, we can optimize the observability using the relative speed and position from row 1 and 3 of columns 1 and 2. This is because only $\nabla\mathcal{L}_f^0 h$ and $\nabla\mathcal{L}_f^1 h$ are needed to construct the observability matrix in Eq. (10) and its accompanying metrics. Then $v_{xr} = u_1 \cos(\psi) - v_{x_{ta}}$ and $v_{yr} = u_1 \sin(\psi) - v_{y_{ta}}$.

E. Gliding Robotic Fish Analysis

Next, we take the model of a gliding robotic fish. Particulars of the robot and its dynamics are described in detail in [22]–[24]. Its state vector $X = [x, y, z, v_1, v_2, v_3, \omega_1, \omega_2, \omega_3, r_{ij}]^T$, consists of the position $b_i = [x, y, z]^T$ of the robot, the 3×3 rotation matrix R from the body frame to the inertial frame with elements r_{ij}, and the body-fixed linear velocity $v_b = [v_1, v_2, v_3]^T$ and angular velocity $\omega_b = [\omega_1, \omega_2, \omega_3]^T$. After replacing the elements of the vector b_i with the relative positions x_r, y_r, and $z_r = z$, the kinematic model is given by

$$\begin{cases} \dot{b}_i = Rv_b - [v_{x_{ta}}, v_{y_{ta}}, 0]^T \\ \dot{R} = R\hat{\omega}_b \end{cases} \tag{19}$$

where $\hat{\omega}_b$ is a skew symmetric matrix ω_b. The structure of the velocity dynamics is given by

$$\begin{bmatrix} \dot{v_1} \\ \dot{v_2} \\ \dot{v_3} \\ \dot{\omega_1} \\ \dot{\omega_2} \\ \dot{\omega_3} \end{bmatrix} = \begin{bmatrix} f_{v11} + a_{v1} r_{31} u_1 + f_{v12} u_3 + f_{v13} u_3^2 \\ f_{v21} + a_{v2} r_{32} u_1 + f_{v21} u_3 + f_{v22} u_3^2 \\ f_{v31} + a_{v3} r_{33} u_1 + f_{v32} u_3 + f_{v33} u_3^2 \\ f_{\omega 11} + f_{\omega 12} u_3 \\ f_{\omega 21} + a_{\omega_2} r_{33} u_2 \\ f_{\omega 31} + a_{\omega_2} r_{32} u_2 + f_{\omega 32} u_3 \end{bmatrix} \tag{20}$$

where u_i are control inputs, a_{v1}, a_{v3} and a_{ω_2} are constants, and f_{vij} and $f_{\omega ij}$ are nonlinear functions of the state vector. The measurement function in this case is actually $h(x) = [||b_i||, z_r, v_1, v_2, v_3, \omega_1, \omega_2, \omega_3, r_{ij}]$. Replacing $||b_i||$ with $||b_i||^2$ and constructing the observability matrix leads to

$$\mathcal{O} = \begin{bmatrix} \nabla\mathcal{L}_f^0 h \\ \nabla\mathcal{L}_f^1 h \end{bmatrix}$$

with

$$\nabla\mathcal{L}_f^0 = \begin{pmatrix} x_r & y_r & z_r & \dots \\ 0 & 0 & 1 & \dots \\ 0 & 0 & 0 & I_{15} \end{pmatrix}$$

$$\nabla\mathcal{L}_f^1 = \begin{pmatrix} \sum_{i=1}^3 r_{1i} v_i - v_{x_{ta}} & \sum_{i=1}^3 r_{2i} v_i - v_{y_{ta}} & \sum_{i=1}^3 r_{3i} v_i & \dots \\ 0 & 0 & 0 & \dots \\ \vdots & \vdots & \vdots & \vdots \\ 0 & 0 & 0 & \dots \end{pmatrix}$$

Because z_r and other state variables are measured, the columns associated with them are all linearly independent and will not cause the observability matrix to lose rank. However, the columns associated with the planar position are not gauranteed to have full rank. In this case, the only non-zero rows can be compressed as

$$\mathcal{O}_p = \begin{bmatrix} x_r & y_r \\ \sum_{i=1}^3 r_{1i} v_i - v_{x_{ta}} & \sum_{i=1}^3 r_{2i} v_i - v_{y_{ta}} \end{bmatrix} \tag{21}$$

This is the same as the observability matrix $\mathcal{O}_p$ in section III-B with $v_{xr} = \sum_{i=1}^3 r_{1i} v_i - v_{x_{ta}}$ and $v_{yr} = \sum_{i=1}^3 r_{2i} v_i - v_{y_{ta}}$. Like the unicycle model, $\nabla\mathcal{L}_f^2$ and beyond will show the functions of the input in these columns, but these are system-specific and much more complicated functions that are not as straightforward to find conditions for making the observability matrix retain full rank. On the other hand,$\nabla\mathcal{L}_f^0$ and $\nabla\mathcal{L}_f^1$ are sufficient to construct the observability metrics $O_1(-C^{-1})$ and $O_2(-\det(\mathcal{O}_p)^2)$.

IV. Simulation Study

A. Unicycle Example

In simulation, the target is represented by a predefined time-dependent trajectory $(x_{ta}(t), y_{ta}(t))$. The range between the target and the unicycle, and the unicycle heading are measured. The measurements are corrupted with additive, zero mean, Gaussian noise and an EKF is used to estimate the position. For fair comparison between the different cases, the noise distribution is held constant for each simulation by setting the random number generator. The optimization problem in Eq. (4) is then solved using the MATLAB nonlinear model predictive control toolbox [25]. The controller uses the estimated position along with the measurement of the other state (heading) as feedback. We assume that the future target trajectory is known over the optimization horizon of 1 second with a 0.2 s time step and that the unicycle's initial state is known. The unicycle has a maximum velocity (u_1) of $0.3\frac{m}{s}$ to mimic the speeds of underwater gliders and limited turn rate (u_2) of $\frac{\pi}{4}\frac{\text{rad}}{s}$. Inputs have rate constraints of

$|\dot{u}_1| < 0.1\frac{m}{s^2}$ and $|\dot{u}_2| < \frac{\pi}{6}\frac{\text{rad}}{s^2}$. For analysis, we show plots of the paths produced along with tables giving statistics on the norm of the estimation error, given by the difference between the true position and EKF estimate, and the norm of the tracking error τ_e as defined in Eq. (1).

TABLE I

SIMULATION RESULTS BASED ON OBSERVABILITY METRIC O_1 (NAMELY, $-C^{-1}$) WITH UNICYCLE MODEL AND STATIC TARGET

		α =0.02	α =0.05	α =0.5
estimation error (m)	max	0.6366	0.4996	0.3530
estimation error (m)	mean	0.1413	0.1492	0.0518
tracking error (m)	min	0.3012	0.2979	0.2557
tracking error (m)	mean	2.0173	2.2304	0.9942

Figure 1 shows the resultant paths taken by the unicycle tracking a static target using $O = O_1$ (namely,$-C^{-1}$) and Table I shows the associated statistics for the norm of the estimation and tracking errors. Because the inverse condition number is upper-bounded by 1, α needs to be fairly small ($\ll$ 1) in order to have an effect when the distance is large. This can be seen with the difference in trajectories produced. When the tracking error and inverse condition number are equally weighted, the unicycle follows a straight line to the target initially. Though the unicycle is able to quickly approach the target and estimate its position well, this behavior could pose a problem if the initial position is inaccurate or the estimate diverges before the tracking error is small enough for the observability metric to influence the control behavior. When the weight α is small, the initial trajectory goes outward before closing in and circling the target. Placing more emphasis on the tracking error (larger α) leads to faster convergence to the target in time. Table I shows that increasing α leads to a smaller average and minimum tracking error. It also shows that, counterintuitively, the estimation error is smaller when the tracking error and the metric are equally weighted. This is likely due to the fact that smaller range generally leads to better estimation performance. In addition, the unicycle spends more time in its performing the circling behavior.

TABLE II

SIMULATION RESULTS BASED ON OBSERVABILITY METRIC O_2 (NAMELY, $-\det(\mathcal{O}_p)^2$) WITH UNICYCLE MODEL AND STATIC TARGET

		α =0.3	α =0.4	α =0.5
estimation error (m)	max	0.6783	0.7746	1.5059
estimation error (m)	mean	0.2230	0.2391	0.2808
tracking error (m)	min	0.0594	0.0055	0.0039
tracking error (m)	mean	3.3466	2.1224	1.8357

Figure 2 shows the resultant paths taken by the unicycle tracking a static target using $O = O_2$ (namely, $-\det(\mathcal{O}_p)^2$). This metric scales with the tracking error, so α can be much closer to equally weighted. Small changes away from equal importance can drastically change the vehicle behavior compared to the metrics. This has the added benefit, that it will not be dominated by the tracking error as a consequence

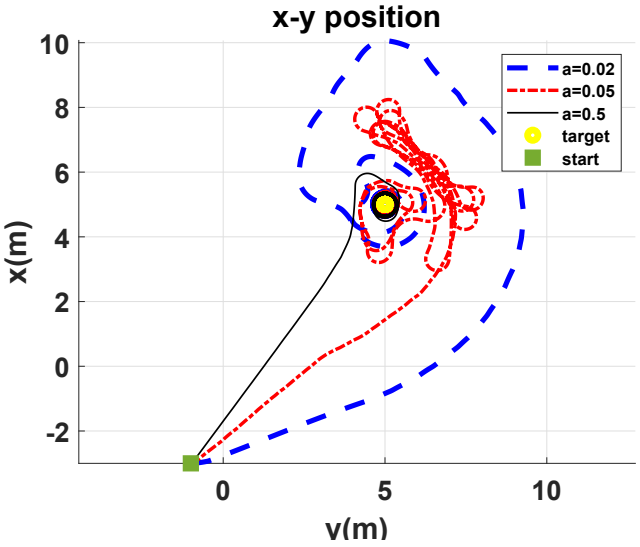

Fig. 1. Paths generated from tracking a static target by optimizing problem (II) with $O = O_1$ (namely, $-C^{-1}$) and weight parameter of 0.5 (solid black), 0.05 (red dash dot), and 0.02 (blue dashed), for the unicycle example.

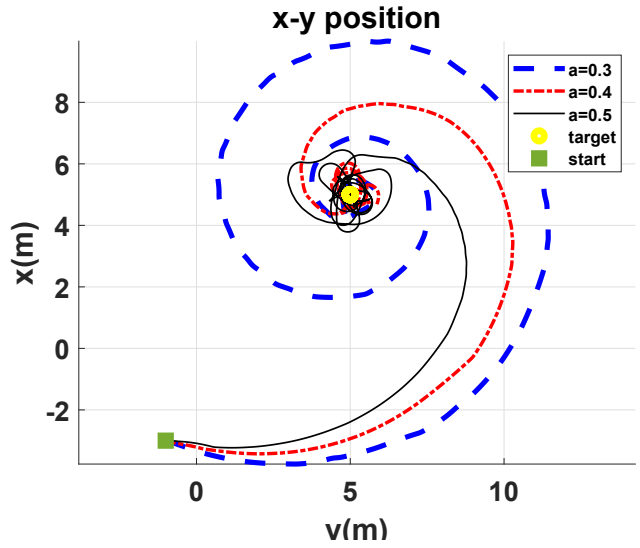

Fig. 2. Paths generated from tracking a static target by optimizing problem (II) with $O = O_2$ (namely, $-\det(\mathcal{O}_p)^2$) and weight parameter of 0.5 (solid black), 0.4 (red dash dot), and 0.3 (blue dashed), for the unicycle example.

of distance, providing a certain robustness, if the position estimation scheme diverges. When this happens, the unicycle will still produce maneuvers that help lower the estimation error. This can be seen by the fact that the unicycle does not travel in a straight-line path even when the two cost elements are equally weighted. It also has the drawback that as the position error shrinks, so does the observability metric. Table II shows that more emphasis on the metric (smaller α) leads to a smaller estimation error, but at the cost of tracking error converging slower.

Figure 3 shows the resultant paths taken by the unicycle tracking a static target using $O = O_3$ (namely, $\text{Tr}(P)$). Like the inverse condition number, O_3 can become overpowered by the tracking error. This behavior could pose a problem

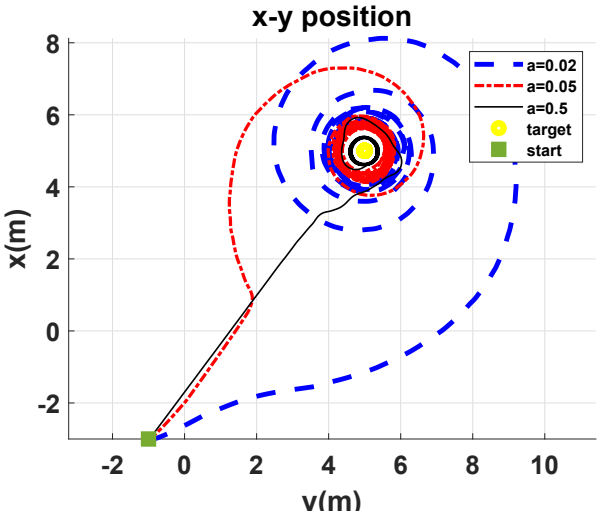

Fig. 3. Paths generated from tracking a static target by optimizing problem (II) with $O = O_3$ (namely, $\mathrm{Tr}(P)$) and weight parameter of 0.5 (solid black), 0.05 (red dash dot), and 0.02 (blue dashed), for the unicycle example.

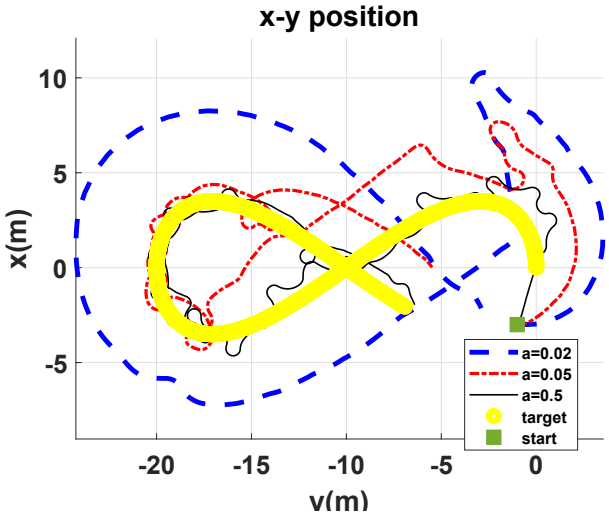

Fig. 4. Paths generated from tracking a static target by optimizing problem (II) with $O = O_1$ (namely, $-C^{-1}$) and weight parameter of 0.5 (solid black), 0.05 (red dash dot), and 0.02 (blue dashed), for the unicycle example.

TABLE III

SIMULATION RESULTS BASED ON OBSERVABILITY METRIC O_3 (NAMELY, $\mathrm{Tr}(P)$) WITH UNICYCLE MODEL AND STATIC TARGET

		α =0.02	α =0.05	α =0.5
estimation error (m)	max	0.3664	0.5093	0.9413
estimation error (m)	mean	0.1197	0.0954	0.0812
tracking error (m)	min	0.6909	0.5119	0.3233
tracking error (m)	mean	2.3329	1.5494	1.0285

if the initial position is inaccurate or the estimate diverges and the tracking error dominates the observability metric. This can be seen when the tracking error and trace of the covariance matrix are equally weighted. The unicycle follows a straight line path until it gets close to the target, which produces a tight circle around the target. When $\alpha \ll 1$, the tracking error converges slower with increasing weight on the observability metric, while the steady-state circling behavior around the target increases in magnitude. Table III shows that larger α leads to a larger maximum estimation error and smaller tracking error.

TABLE IV

SIMULATION RESULTS BASED ON OBSERVABILITY METRIC O_1 (NAMELY, $-C^{-1}$) WITH UNICYCLE MODEL AND MOVING TARGET

		α =0.02	α =0.05	α =0.5
estimation error (m)	max	1.6683	0.9789	0.9435
estimation error (m)	mean	0.6362	0.2265	0.1590
tracking error (m)	min	3.1623	0.1418	0.027
tracking error (m)	mean	5.4270	2.4693	0.9526

Figures 4-6 show the resultant paths taken by the unicycle tracking a moving target using $O = O_1$ (i.e., $-C^{-1}$), $O = O_2$ (i.e., $-\det(\mathcal{O}_p)^2$), and $O = O_3$ (i.e., $\mathrm{Tr}(P)$), respectively. Tables IV-VI show the mean and maximum estimation error and the mean and minimum tracking error for each method. Generally, the data shows a similar trend

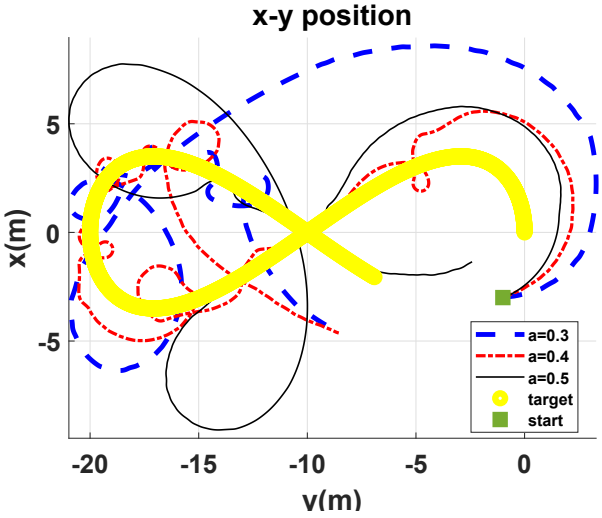

Fig. 5. Paths generated from tracking a static target by optimizing problem (II) with $O = O_2(-\det(\mathcal{O}_p)^2)$ and weight parameter of 0.5 (solid black), 0.05 (red dash dot), and 0.02 (blue dashed), for the unicycle example.

as for the static case. However, using O_3 highlights the potential problem of the tracking objective dominating the observability objective. When equally weighted, the scheme based on O_3 initially tracks the target well, but the estimation and tracking error both diverge and are unable to recover. A similar situation happens for $O = O_2$, but the unicycle is able to keep the error from increasing indefinitely. With $O = O_1$, the unicycle is able to avoid the divergence all together. When more weight is placed on the any of the observability metrics, tracking error grows, but the estimation error is kept low.

B. Gliding Robotic Fish Example

Simulations with the gliding robotic fish are carried out in an identical fashion to that of the unicycle with the exception of system being used to track the target. Figure 7 and Table

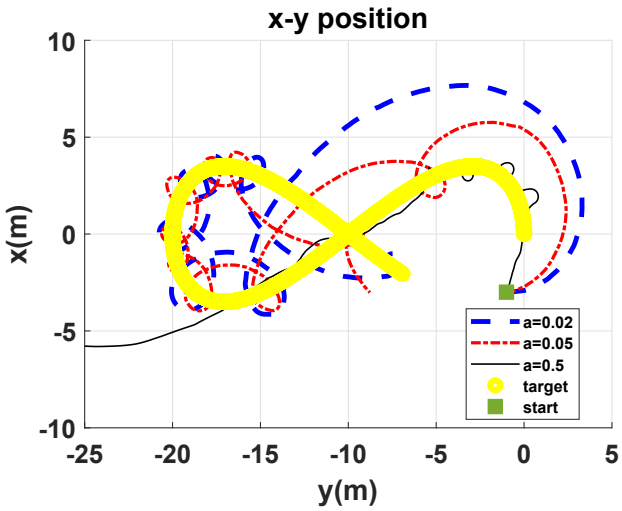

Fig. 6. Paths generated from tracking a moving target by optimizing problem (II) with $O = O_3(\mathrm{Tr}(P))$ and weight parameter of 0.5 (solid black), 0.05 (red dash dot), and 0.02 (blue dashed), for the unicycle example.

TABLE V

SIMULATION RESULTS BASED ON OBSERVABILITY METRIC O_2 (NAMELY, $-\det(\mathcal{O}_p)^2$) WITH UNICYCLE MODEL AND MOVING TARGET

		α =0.3	α =0.4	α =0.5
estimation error (m)	max	1.4734	2.2962	6.9132
estimation error (m)	mean	0.3542	0.5762	2.2937
tracking error (m)	min	0.0827	0.3646	0.2188
tracking error (m)	mean	3.5718	1.7745	4.12

TABLE VI

SIMULATION RESULTS BASED ON OBSERVABILITY METRIC O_3 (NAMELY, $\mathrm{Tr}(P)$) WITH UNICYCLE MODEL AND MOVING TARGET

		α =0.02	α =0.05	α =0.5
estimation error (m)	max	0.6449	0.4694	35.9
estimation error (m)	mean	0.1641	0.1277	16.49
tracking error (m)	min	0.4182	0.3646	0.0827
tracking error (m)	mean	2.6441	1.8114	11.22

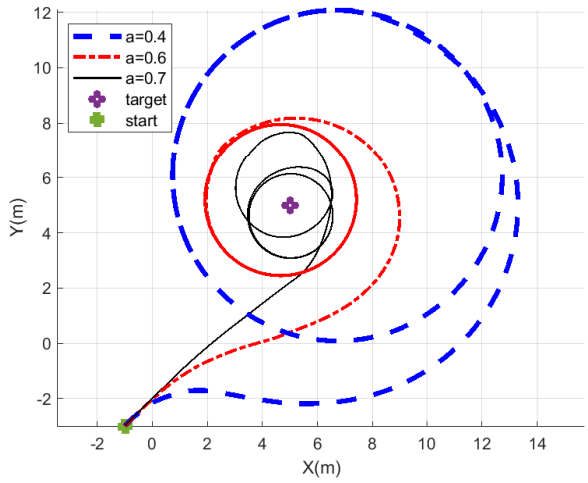

Fig. 7. Paths generated from tracking a static target by optimizing problem (II) with $O = O_2$ (namely, $-\det(\mathcal{O}_p)^2$) and robotic fish model. Weight parameters are of 0.4 (solid black), 0.6 (red dash dot), and 0.7 (blue dashed), for robotic fish example.

VIII show the resultant path for the gliding robotic fish model, tracking error statistics, and estimation error statistics when problem (4) is solved using $O = O_2$. Though the glider moves in three dimensions, we still only consider the tracking error τ_e defined in (1). The planar paths are qualitatively similar to that of the unicycle model, but the weight parameter has a much larger effect on the minimum distance to the target. Another difference from the unicycle results is that the target is not at the center of the steady-state circular behavior. The trend of the tracking error also follows a similar pattern. The estimation error, however, does not. This is likely due to the fact that higher weight on the tracking error allows the robot to get closer to the target which generally provides better estimation error so long as the relative position is not zero.

Figure 8 and Table VII show the resultant path for the gliding robotic fish model, tracking error statistics, and estimation error statistics when problem (4) is solved using $O = O_1$. The paths generated from the inverse condition number all share similar geometry and the asymmetric steady-state behavior around the target is even more drastic. The mean of the tracking error still follows expected trend, but the minimum is skewed by the asymmetry. The estimation error is kept small, but does not follow intuitive trend as in the unicycle example.

V. CONCLUSION AND FUTURE WORK

In this work, we studied the trade-off between observability and control performance for a mobile robot in target tracking, with only distance measurement by jointly optimizing the tracking cost and an observability metric. The trace of the covariance matrix in position estimation, determinant of the observability matrix, and inverse condition number of the observability matrix were chosen as metrics to compare. The pros and cons of each metric were discussed and a relationship was shown between the metrics derived from the observability matrix. Simulation studies were carried out for a unicycle model and the dynamics of a gliding robotic fish. All three metrics are shown to be capable of providing satisfactory tracking performance while preventing estimation divergence, when the weights are properly chosen. Investigating the effect of relative importance between tracking performance and observability revealed that care should be taken when using the covariance and the inverse condition number. The weight α should be $\ll 1$ to account for large distances. The determinant scales relative to the tracking error and will work for arbitrary distance when equally weighted.

In the future, we plan to study the feasibility of this method when taking into account the delays in communication and range measurements. We also plan to identify more efficient solutions to enable real-time implementation when dealing

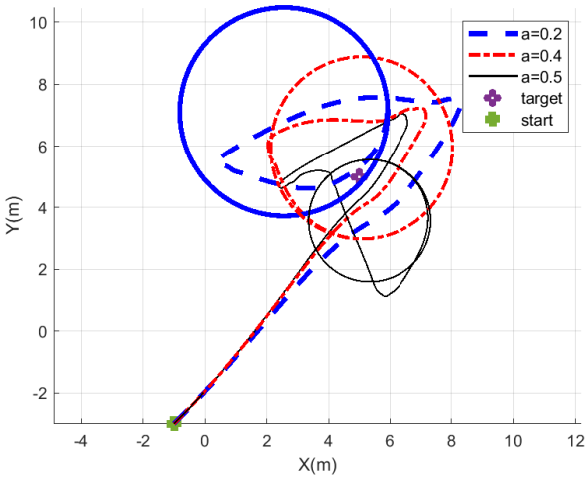

Fig. 8. Paths generated from tracking a static target by optimizing problem (II) with $O = O_1$ (namely, $-C^{-1}$) and robotic fish model. Weight parameters are of 0.5 (solid black), 0.4 (red dash dot), and 0.2 (blue dashed), for robotic fish example.

TABLE VII

SIMULATION RESULTS BASED ON OBSERVABILITY METRIC O_1 (NAMELY, $-C^{-1}$) WITH GLIDING ROBOTIC FISH MODEL AND STATIC TARGET

		α =0.4	α =0.6	α =0.7
estimation error (m)	max	0.4116	0.4730	.3709
estimation error (m)	mean	0.1734	0.1012	.1758
tracking error (m)	min	0.1475	0.8437	0.5170
tracking error (m)	mean	4.1080	3.4323	2.8236

with richer dynamical systems such as the gliding robotic fish. Finally, field experiments involving an autonomous surface vehicle and a gliding robotic fish will be conducted to validate the findings in this work.

TABLE VIII

SIMULATION RESULTS BASED ON OBSERVABILITY METRIC O_2 (NAMELY, $-\det(\mathcal{O}_p)^2$) WITH GLIDING ROBOTIC FISH MODEL AND STATIC TARGET

		α =0.2	α =0.4	α =0.5
estimation error (m)	max	0.6353	0.3757	.6091
estimation error (m)	mean	0.1204	0.1337	.1092
tracking error (m)	min	3.9519	2.3574	1.1152
tracking error (m)	mean	6.8256	3.6380	2.4190

REFERENCES

[1] J. Wu, R. C. Bingham, S. Ting, K. Yager, Z. J. Wood, T. Gambin, and C. M. Clark, "Multi-AUV motion planning for archeological site mapping and photogrammetric reconstruction," *Journal of Field Robotics*, vol. 36, no. 7, pp. 1250–1269, 2019.

[2] S. B. Williams, O. Pizarro, M. Jakuba, and N. Barrett, "AUV benthic habitat mapping in south eastern tasmania," in *Field and Service Robotics*. Springer, 2010, pp. 275–284.

[3] H. Stommel, "The Slocum Mission," *Oceanography*, vol. 2, no. 1, pp. 22–25, 1989.

[4] J. Sherman, R. E. Davis, W. Owens, and J. Valdes, "The autonomous underwater glider "Spray"," *IEEE Journal of Oceanic Engineering*, vol. 26, no. 4, pp. 437–446, 2001.

[5] J. Sliwka, B. Clement, and I. Probst, "Sea glider guidance around a circle using distance measurements to a drifting acoustic source," in *Intelligent Robots and Systems (IROS), 2012 IEEE/RSJ International Conference on*. IEEE, 2012, pp. 94–99.

[6] L. Paull, S. Saeedi, M. Seto, and H. Li, "AUV navigation and localization: A review," *IEEE Journal of Oceanic Engineering*, vol. 39, no. 1, pp. 131–149, 2013.

[7] A. S. Gadre and D. J. Stilwell, "A complete solution to underwater navigation in the presence of unknown currents based on range measurements from a single location," in *2005 IEEE/RSJ International Conference on Intelligent Robots and Systems*. IEEE, 2005, pp. 1420–1425.

[8] Q. Chen, K. You, and S. Song, "Cooperative localization for autonomous underwater vehicles using parallel projection," in *2017 13th IEEE International Conference on Control & Automation (ICCA)*. IEEE, 2017, pp. 788–793.

[9] A. Bahr, J. J. Leonard, and M. F. Fallon, "Cooperative localization for autonomous underwater vehicles," *The International Journal of Robotics Research*, vol. 28, no. 6, pp. 714–728, 2009.

[10] Y. Huang, Y. Zhang, B. Xu, Z. Wu, and J. A. Chambers, "A new adaptive extended Kalman filter for cooperative localization," *IEEE Transactions on Aerospace and Electronic Systems*, vol. 54, no. 1, pp. 353–368, 2017.

[11] M. F. Fallon, G. Papadopoulos, J. J. Leonard, and N. M. Patrikalakis, "Cooperative AUV navigation using a single maneuvering surface craft," *The International Journal of Robotics Research*, vol. 29, no. 12, pp. 1461–1474, 2010.

[12] P. Baccou and B. Jouvencel, "Homing and navigation using one transponder for AUV, postprocessing comparisons results with long base-line navigation," in *Proceedings 2002 IEEE International Conference on Robotics and Automation (Cat. No. 02CH37292)*, vol. 4. IEEE, 2002, pp. 4004–4009.

[13] B. T. Hinson, M. K. Binder, and K. A. Morgansen, "Path planning to optimize observability in a planar uniform flow field," in *2013 American Control Conference*. IEEE, 2013, pp. 1392–1399.

[14] A. Ross and J. Jouffroy, "Remarks on the observability of single beacon underwater navigation," in *Proc. Intl. Symp. Unmanned Unteth. Subm. Tech*, 2005.

[15] G. Antonelli, F. Arrichiello, S. Chiaverini, and G. S. Sukhatme, "Observability analysis of relative localization for AUVs based on ranging and depth measurements," in *2010 IEEE International Conference on Robotics and Automation*. IEEE, 2010, pp. 4276–4281.

[16] F. Arrichiello, G. Antonelli, A. P. Aguiar, and A. Pascoal, "An observability metric for underwater vehicle localization using range measurements," *Sensors*, vol. 13, no. 12, pp. 16 191–16 215, 2013.

[17] M. Rafieisakhaei, S. Chakravorty, and P. Kumar, "On the use of the observability gramian for partially observed robotic path planning problems," in *2017 IEEE 56th Annual Conference on Decision and Control (CDC)*. IEEE, 2017, pp. 1523–1528.

[18] B. Ferreira, A. Matos, and N. Cruz, "Single beacon navigation: Localization and control of the MARES AUV," in *OCEANS 2010 MTS/IEEE SEATTLE*. IEEE, 2010, pp. 1–9.

[19] J. D. Quenzer and K. A. Morgansen, "Observability based control in range-only underwater vehicle localization," in *2014 American Control Conference*. IEEE, 2014, pp. 4702–4707.

[20] X. S. Zhou and S. I. Roumeliotis, "Robot-to-robot relative pose estimation from range measurements," *IEEE Transactions on Robotics*, vol. 24, no. 6, pp. 1379–1393, 2008.

[21] R. Hermann and A. Krener, "Nonlinear controllability and observability," *IEEE Transactions on Automatic Control*, vol. 22, no. 5, pp. 728–740, 1977.

[22] D. Coleman, M. Castanon, and X. Tan, "Backstepping-based trajectory tracking for underwater gliders," in *ASME 2019 Dynamic Systems and Control Conference*. American Society of Mechanical Engineers Digital Collection, 2019, paper 9028.

[23] F. Zhang, "Modeling, design and control of gliding robotic fish," Dissertation, Michigan State University. Electrical Engineering, 2014.

[24] D. Coleman and X. Tan, "Backstepping control of gliding robotic fish for trajectory tracking in 3D space," in *2020 American Control Conference (ACC)*. IEEE, 2020, pp. 3730–3736.

[25] "Matlab optimization toolbox," 2020.